Journal of ELECTRONIC MATERIALS
DOI: 10.1007/s11664-017-5380-5

Systematics of Structural, Phase Stability, and Cohesive Properties of η'-$Cu_6(Sn,In)_5$ Compounds Occurring in In-Sn/Cu Solder Joints

S.B. RAMOS,[1,2,8] N.V. GONZÁLEZ LEMUS,[1,2] C.E. DELUQUE TORO,[3] G.F. CABEZA,[4,5] and A. FERNÁNDEZ GUILLERMET[6,7]

1.—Facultad de Ingeniería, Universidad Nacional del Comahue, Buenos Aires 1400, 8300 Neuquén, Argentina. 2.—Instituto de Investigación y Desarrollo en Ingeniería de Procesos, Biotecnología y Energías Alternativas, CONICET-UNCo, Neuquén, Argentina. 3.—Grupo de Nuevos Materiales, Facultad de Ingeniería, Universidad del Magdalena, Carrera 32 No. 22-08, Santa Marta, Colombia. 4.—Departamento de Física, Universidad Nacional del Sur, Bahía Blanca, Argentina. 5.—Instituto de Física, UNS - CONICET, Bahía Blanca, Argentina. 6.—Centro Atómico Bariloche e Instituto Balseiro, Avda. Bustillo 9500, 8400 Bariloche, Argentina. 7.—CONICET, Buenos Aires, Argentina. 8.—e-mail: susana.ramos@fain.uncoma.edu.ar

Motivated by the high solubility of In in (*mC44*) η'-Cu_6Sn_5 compound as well as the occurrence of an In-doped η'-intermetallic in the microstructure of Cu/In-Sn/Cu solder joints, a theoretical study has been carried out to investigate the various physical effects of incorporating In at Sn Wyckoff sites of the binary η'-phase. Systematic *ab initio* calculations using the projected augmented wave method and Vienna *Ab initio* Simulation Package were used to determine the composition dependence of the structural and cohesive properties of η'-$Cu_6(Sn,In)_5$ compounds, compared with those expected from the binary end-member compounds Cu_6Sn_5 and Cu_6In_5. The molar volume shows significant deviations from Vegard's law. The predicted composition dependence of the cohesive properties is discussed using two complementary approaches, viz. a valence-electron density approach as well as a bond-number approach, both accounting for the roughly linear dependence of the cohesive energy on the In content. A microscopic interpretation for this general trend is given in terms of the key contributions to chemical bonding in this class of compounds, namely Cu *d*-electron overlap and hybridization of Cu *d*-states with In and Sn *p*-electron states. Moreover, a crystallographic site approach is developed to accurately establish the phase-stabilizing effect of incorporating In at specific Wyckoff positions of the (*mC44*) η'-Cu_6Sn_5 structure.

Key words: Lead-free soldering alloys, *ab initio* calculations, cohesive properties, phase stability, electronic structure, Cu–In–Sn intermetallic compounds

INTRODUCTION

Traditionally, Pb–Sn solders have been used as the most important materials for modern electronic components and devices. More recently, emerging environmental regulations, in particular in Europe and Japan, have targeted elimination of Pb usage due to its toxicity. This has encouraged extensive research on Pb-free solders for electronic packaging applications.[1] Most candidate lead-free solders are based on Sn with two or more major alloying elements. Among them, In-48 at.%Sn eutectic alloy has long been considered a very attractive alternative, since it has low melting point (120°C), high ductility, long fatigue life, and excellent wettability.[2]

(Received July 19, 2016; accepted February 15, 2017)

Published online: 20 March 2017

For all solder technologies, the chemical interaction between the solder and the metal substrate is of great importance. During soldering, some of the base metal with which the joint is formed is dissolved into the molten solder. As a result, the solder becomes supersaturated with the dissolved metal and an intermetallic compound (IMC) layer precipitates on the metal surface.[3] Consequently, in any solder joint, a layer of at least one intermetallic compound (IMC) is present between the solder and substrate. The presence of a thin, continuous, uniform IMC layer between the solder and conductor metals is an indication of good metallurgical bonding. However, due to their inherently brittle nature and tendency to generate structural defects, a thick IMC layer may degrade solder joint reliability.[4] In some cases, the intermetallic layer may consist of two IMCs, with compositions depending upon the combination of metal substrate and solder used. From the metallurgical viewpoint, knowledge of solder/substrate chemical interactions and phase evolution is important for understanding and controlling interconnection reliability.[3]

Since Cu is the most commonly used contact material, there has long been fundamental and technological interest in study of the IMCs formed by the reaction between Sn-based solder and Cu substrate. Extensive experimental work reported in recent decades[3,5–15] indicates that such reaction forms, in the first place, a compound with formula Cu_6Sn_5.

Cu_6Sn_5 IMC originates in the Cu–Sn system, where it occurs with two structures: monoclinic (*mC44*) phase, usually denoted as η'-Cu_6Sn_5, stable at temperatures lower than about 186°C,[16] and hexagonal ($P6_3/mmc$) η-Cu_6Sn_5 phase, stable at higher temperatures.[17] Both η and η' are reported to be nonstoichiometric, and their stability range might enable crystal structure variations.[18] The high-temperature η-phase field has been systematically studied by Larsson et al.,[16] and two superstructures have been found, namely η^6 and η^8. In fact, recent work refers to up to five crystal structures, whose occurrence seems to depend upon compositional variations and the processing route applied.[19]

Various features of the behavior of η- and η'-IMCs and their transformation, which are of technological importance, are reviewed below in the framework of the motivations for the present work.

First, the η-to-η' phase transition is accompanied by an increase in volume of about 2%.[20] Under service conditions, such a volume change would produce an important stress concentration and possibly cause solder interconnect failure. The time available during soldering and subsequent cooling is insufficient for the η'-to-η transformation, thus the high-temperature η-Cu_6Sn_5 phase might remain as a metastable phase.[3] If the service temperature is near room temperature, such transformation does not occur within a reasonable time, because of kinetic constraints. However, at temperatures around 150°C, which might be reached, e.g., because of local heating caused by use of power components, this transformation occurs in relatively short times.[3]

Second, it has long been accepted that the formation of Cu_6Sn_5 (and other IMCs) in solder joints plays an important role in their long-term reliability.[21] Cu_6Sn_5 phase is formed instantly by liquid-state diffusion during the soldering process, whereas subsequent exposure to thermal cycling aging causes the IMC layer to grow by solid-state diffusion.[3,7,8] This is expected to degrade the mechanical properties after exposure to thermal cycling aging, in particular the residual shear and fatigue strength.[8,22,23] Moreover, formation of IMCs is important in that these phases are generally considered stiffer and more brittle than bulk solder, which could make the solder joint brittle and eventually lead to cracking even at lower loads than expected.[4]

More recently, study of the effects of IMC formation on the microstructure and reliability of solder joints of interest for development of microelectronic devices, photovoltaic systems, and other advanced applications has been facilitated by the introduction of the synchrotron x-ray microdiffraction (μXRD) technique,[24–29] which allows characterization of a crystalline material in small, localized volumes and study of stress and microstructure evolution, e.g., during and after annealing or thermal cycling. This technique can detect even trace amounts and identify the IMCs present in a solder joint. In particular, application of μXRD for characterization of the stress and microstructure evolution in solder joints of crystalline Si solar cells indicates absence of IMCs in fresh samples obtained from the solder joint, and that Cu_6Sn_5 forms after thermal cycling due to activated interdiffusion of Cu and Sn. Moreover, scanning electron microscopy observations on thermally cycled samples show that cracks form in the bulk solder.[25]

Third, the possible use of alloying to control the volume change in the η-to-η' transformation (and other undesirable effects) has motivated renewed experimental and theoretical interest in the structural, mechanical, and phase stability properties of ternary IMCs formed by incorporating a third element into binary Cu_6Sn_5 phase. Experimental studies have shown, in particular, that dissolution of Ni into the binary compound can suppress η-to-η' transformation on cooling, leading to stabilization of the hexagonal η'-phase to room temperature.[20,30] Additions of other elements soluble in Cu_6Sn_5, such as Zn, Au, and In, have also been shown experimentally to prevent the hexagonal-to-monoclinic transition.[31] In turn, these experimental findings have stimulated very recent *ab initio* density functional theory (DFT) studies of incorporation of various elements into binary Cu_6Sn_5 phase. In particular, Gao et al.[32] investigated the effects of

adding Ni or Co atoms into the (*mC44*) Cu_6Sn_5 compound. Using DFT calculations of the energy of formation, they found that these dopants increased the stability of the respective $(Cu,Ni)_6Sn_5$ and $(Cu,Co)_6Sn_5$ phases with respect to the binary compound, and determined the most favorable occupancy sites for Ni and Co. Moreover, by analyzing the electronic density of states (DOS), they concluded that hybridization between Ni *d*- (or Co *d*-) and Sn *p*-states plays a dominant role in the stability of these structures.[32] Zhang et al.[33] also used DFT calculations to study the stability and mechanical properties of (η')-Cu_6Sn_5 doped with Ni, Au, Zn, and In. They found that the phase stability and mechanical properties could be enhanced by doping these elements, in particular Ni.

This literature review indicates that there is abundant information on the properties of Cu–Sn–X ternary high-temperature η-Cu_6Sn_5 phases, but considerably less work has been reported on the effects of incorporating a third element into the low-temperature η'-Cu_6Sn_5 phase. Such incorporation is the theme of the present work. Specifically, the current study focuses on the most general physical effects of adding In into the binary η'-Cu_6Sn_5 phase. This work has several motivations, which are presented below.

The first motivation is the extensive solubility of In in the Cu_6Sn_5 phase, a feature already present in the early Cu–Sn–In phase diagram[34] that has recently been corroborated by neutron diffraction experiments.[35,36] The second motivation is the well-documented occurrence of In-doped Cu_6Sn_5 IMCs in the microstructure of In-Sn/Cu solder joints. For instance, Kim and Jung[37] reported that two IMCs formed at the interface during aging at temperatures between 70°C and 100°C, namely ε-$Cu(In,Sn)_2$, adjacent to the solder, and $Cu_6(Sn,In)_5$, adjacent to the Cu substrate, which was the dominant phase. Chuang et al.[9] reported that a planar layer of $Cu_3(Sn,In)$ at the Cu side and a scalloped layer of $Cu_6(Sn,In)_5$ at the solder side were formed at the eutectic In-Sn/Cu interface during reflow at temperatures ranging from 150°C to 400°C. Sommadossi and Fernández Guillermet[38] studied the interconnection zone in Cu/In-Sn/Cu diffusion-soldering joints. In samples annealed at 220°C for 436 h, they found ternary η-phases with compositions changing between those corresponding to the ideal formulas $Cu_6(Sn,In)_5$ and $Cu_2(In,Sn)$.

The third motivation for the present work is the fact that current DFT calculations suggest that addition of In has a relatively small suppressive effect on the η-to-η' transformation.[33] This fact points to the importance of detailed characterization of the η'-phase, which is the equilibrium structure at low temperatures.

A fourth, theoretical motivation for this study is the long-standing interest in thermodynamic modeling of nonstoichiometric multicomponent IMCs characterized by various crystallographic sublattices.[39] Towards that aim, it is necessary to know the most probable distribution of alloying elements at available crystallographic sites. Such information is usually not available from experiments.[34,36]

The current work continues a line of research aimed at characterizing a large family of IMCs formed when soldering In-Sn alloy with Cu and Ni, the commonest substrates. Motivated by the general need for physicochemical information on these technically relevant materials, the present authors previously focused on theoretical predictions, systematization, and interpretation in microscopic terms of properties of the IMCs which are stable or metastable in the binary subsystems of the quaternary (Cu,Ni)–(In,Sn) system. Specifically, information on the lattice parameters and cell volume, bulk modulus, and other equation-of-state parameters, as well as the energy of formation from the elements and the electronic structure of several Cu–In,[40,41] Cu–Sn,[40] Ni–In, and Ni–Sn[42,43] stoichiometric IMCs was obtained by *ab initio* projected augmented wave (PAW) calculations[44,45] using the Vienna *Ab initio* Simulation Package (VASP).[46] By extending this line of research, the general aim of the present work is to perform a systematic study of the structural, cohesive, and electronic structure effects of incorporating various amounts of In into the structure of the η'-Cu_6Sn_5 (*mC44*) IMC. The specific purposes of this work are listed below:

First, we aim to establish an energetically favorable way in which In atoms can replace Sn atoms originally located at various crystallographic sublattices of the binary (*mC44*) phase. This issue is addressed by evaluating and comparing the energy effects involved in progressive filling with In at crystallographic sites originally occupied by Sn. Second, we aim to study the effects of In addition upon the lattice parameters, cell volume, and bulk modulus of $Cu_6(Sn,In)_5$ phase. Third, we aim to produce a unified picture of the cohesive behavior of the $Cu_6(Sn,In)_5$ compounds, relying upon the correlation procedures previously applied to (Cu,Ni)–(In,Sn) lead-free soldering IMCs.[47] Once the cohesive properties have been systematized, microscopic interpretation of the theoretical trends will be developed. Specifically, the composition dependence of the electronic structure of the $Cu_6(Sn,In)_5$ compounds will be discussed in the light of current theories of chemical bonding for the present class of IMCs.

PHASES, STRUCTURES, AND THEORETICAL METHOD

The present theoretical method was described elsewhere.[40–43,47,48] In the following, we summarize only the points of relevance for the present study. We performed total-energy DFT calculations using the PAW method[44,45] and VASP code.[46] We used the generalized gradient approximation (GGA) to

evaluate the exchange–correlation energy, with the functions given by Perdew and Wang (GGA-PW91).[49] The valence electrons involved in the calculations are 11 for Cu ($3d^{10}4s^1$), 3 for In ($5s^2p^1$), and 4 for Sn ($5s^2p^2$). The cutoff energy for the PAW potential is 314 eV, leading to total energies and cohesive energies converged within 10 meV/atom and 2 meV/atom, respectively.

The Brillouin zone is mapped using the Monkhorst–Pack method, with a **k**-point mesh[50] of $5 \times 7 \times 5$ found sufficient to achieve well-converged energies (within 1 meV/atom). For occupation of the electronic levels, the step function is replaced by a smooth function more appropriate for a metallic system. Here, we use the Methfessel–Paxton technique in which the step function is expanded in a complete set of orthogonal functions, with electrons at some finite temperature given through the smearing factor $\sigma = k_B T = 0.1$.[51] The zeroth-order Methfessel–Paxton function corresponds to simple, Fermi–Dirac-like smearing. The lattice parameters and ionic degrees of freedom were relaxed until the forces on the ions were lower than 30 meV/Å. The cohesive energy and the energy of formation per atom for each of the $Cu_6(Sn,In)_5$ IMCs studied were calculated following the usual procedure.[48,52] The calculation of the cohesive energy involves evaluation of the total energy of the isolated Cu, In, and Sn atoms, whereas the calculation of the energy of formation requires that of the elements in their equilibrium phases, viz. fcc (Cu), tI2 (In), and tI4 (Sn).[40]

The (*mC44*) η'-Cu_6Sn_5 structure, presented in Fig. 1, consists of four Cu sublattices with Wyckoff symmetric positions 4a (Cu1), 4e (Cu2), 8f (Cu3), and 8f (Cu4) for Cu atoms, and 4e (Sn1), 8f (Sn2), and 8f (Sn3) for Sn atoms.[40] The last two Sn-8f sublattices will be referred to in the remainder of the paper as $8f_1$ and $8f_2$, respectively. These various Wyckoff sites are indicated in Fig. 1.

To model the ternary $Cu_6(In,Sn)_5$ compounds, the Sn atoms are progressively replaced by In atoms, occupying the three Wyckoff positions of the Sn atoms, and their combinations, to form the eight hypothetical compounds listed in Table I and labeled I to VIII. For each of these structures, we established the cohesive energy, energy of formation, lattice parameters and internal coordinates, equilibrium volume, bulk modulus, and electronic density of states.

RESULTS

The calculated lattice parameters, equilibrium volume per atom, bulk modulus, and cohesive energy for the elements Cu, In, and Sn in their known equilibrium structures were reported elsewhere.[40,47] These results compare very well with the available experimental data[53–59] and with other *ab initio* calculations.[60] Such agreement adds to our confidence in the present theoretical technique. In the following, we present and discuss the results for the η'-$Cu_6(Sn,In)_5$ compounds.

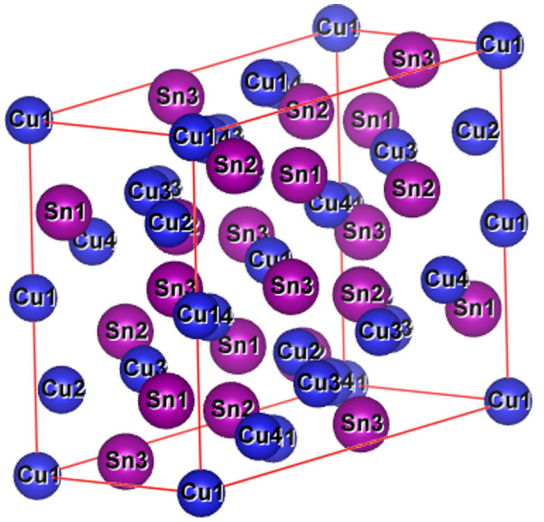

Fig. 1. Structure of η'-Cu_6Sn_5 phase. The different atomic sublattice Wyckoff positions are indicated, on the basis of experimental information given in Ref. 53.

Table I presents the lattice parameters (a, b, and c), average volume per atom (V_0), bulk modulus (B_0), energy of formation from the elements (EOF), and cohesive energy (E_{coh}) of the eight (*mC44*) η'-$Cu_6(Sn,In)_5$ compounds considered. Each one of these IMCs is represented by a formula (with 44 atoms) of type $Cu_{24}(Sn,In)_4(Sn,In)_8(Sn,In)_8$, indicating that 24 Cu atoms are placed at 4a, 4e, and two 8f Wyckoff sites, 4 (Sn or In) atoms at 4e sites, 8 (Sn or In) atoms at $8f_1$ sites, and 8 (Sn or In) atoms at $8f_2$ sites. We remark that the binary η'-Cu_6In_5 resulting from complete replacement of Sn by In is not a stable phase in the Cu–In phase diagram.[34,61] However, as we have discussed elsewhere,[40,47] its properties are of great interest in connection with CALPHAD-type[62] thermodynamic modeling of the nonstoichiometric $Cu_6(Sn,In)_5$ phase of the Cu–In–Sn phase diagram using, e.g., the compound energy formalism.[63]

Composition Dependence of Atomic Volume

The composition dependence of V_0 is presented in Fig. 2. The symbols represent the V_0 values corresponding to each of the eight compounds in Table I, while the dashed line describes the values predicted by a linear, Vegard's law-type interpolation between the binary Cu_6Sn_5 and Cu_6In_5 phases, usually referred to as end-member compounds (EMCs). At each In atomic composition, when more than one possibility of Sn sublattice replacement exists, the empty symbols correspond to the compounds with higher energies of formation. When passing from Cu_6Sn_5 to Cu_6In_5, the average volume per atom decreases. The V_0 versus at.% In plot shows negative deviations from Vegard's law in the range

Table I. Crystallographic site occupations, In content in the η'-$Cu_6(Sn,In)_5$ compound, lattice parameters in Å, equilibrium volume (V_0) in Å^3/atom, bulk modulus (B_0) in GPa, cohesive energy (E_{coh}) in kJ/mol-atom, and energy of formation (EOF) in kJ/mol-atom

	Formula	Crystallographic Site Occupation 4a	4e	8f	8f	4e	$8f_1$	$8f_2$	% In	a, b, c (Å)			β	V_0 (Å^3/atom)	B_0 (GPa)	E_{coh} (kJ/mol)	EOF (kJ/mol)
I	$Cu_{24}Sn_4Sn_8Sn_8$	Cu	Cu	Cu	Cu	Sn	Sn	Sn	0	11.134	7.404	9.989	98.706	18.428	80.900	329.060	−3.350
										(11.036	7.288	9.841	98.810	17.777)[a]	84.400[b]		
										11.138	7.403	9.995	98.650	18.512	79.600		−3.205[c]
										(11.119	7.384	9.948	98.730	18.347	77.600		−3.780)[d]
II	$Cu_{24}In_4Sn_8Sn_8$	Cu	Cu	Cu	Cu	In	Sn	Sn	20	11.130	7.404	9.840	99.028	18.200	83.300	322.220	−3.445
III	$Cu_{24}Sn_4In_8Sn_8$	Cu	Cu	Cu	Cu	Sn	In	Sn	40	11.142	7.388	9.868	99.163	18.226		314.209	−2.369
IV	$Cu_{24}Sn_4Sn_8In_8$	Cu	Cu	Cu	Cu	Sn	Sn	In	40	11.128	7.362	9.889	98.770	18.196	79.500	315.708	−3.868
V	$Cu_{24}In_4In_8Sn_8$	Cu	Cu	Cu	Cu	In	In	Sn	60	11.123	7.369	9.857	99.413	18.114		307.171	−2.266
VI	$Cu_{24}In_4Sn_8In_8$	Cu	Cu	Cu	Cu	In	Sn	In	60	11.141	7.327	9.891	99.149	18.118	82.100	308.731	−3.826
VII	$Cu_{24}Sn_4In_8In_8$	Cu	Cu	Cu	Cu	Sn	In	In	80	11.178	7.279	9.954	99.463	18.155	79.700	299.538	−1.568
VIII	$Cu_{24}In_4In_8In_8$	Cu	Cu	Cu	Cu	In	In	In	100	11.112	7.308	9.957	99.177	18.070		291.803	−0.778

[a]Experimental data.[3b]Experimental data at 298 K.[39c]*Ab initio* ultrasoft pseudopotential (US-PP) calculated values.[39d]*Ab initio* PAW calculated values.[15]

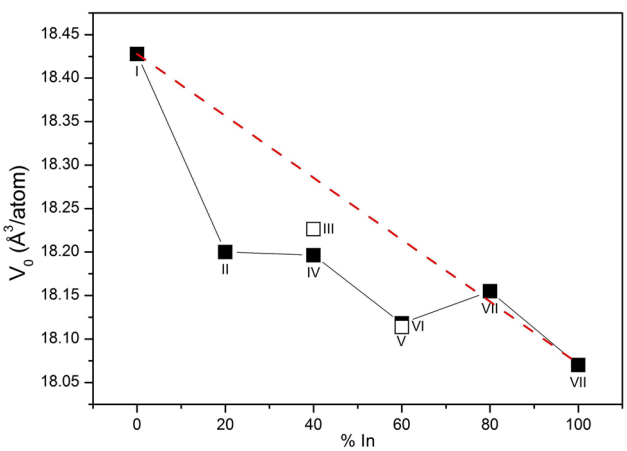

Fig. 2. Composition dependence of average volume per atom of (*mC44*) η'-$Cu_6(Sn,In)_5$ compounds. At each In atomic composition, when more than one possibility of Sn sublattice replacement exists, the empty symbols correspond to the IMCs with higher energies of formation.

0 < at.% In < 80. It was also found that the occupation by In of the $8f_1$ sites in compound III (open symbol) yields a larger volume compared with the $8f_2$ sites in compound IV. On the other hand, the occupation of both the 4e and $8f_1$ sites in compound V (open symbol) leads to a slightly lower volume than the 4e and $8f_2$ sites in compound VI.

Comparison with previous results can only be made for the Cu_6Sn_5 compound. Table I indicates that the present V_0 value (18.428 Å^3/atom) is about 3.7% larger than the experimental value.[16] Such discrepancy is comparable to other results in literature obtained using the present theoretical method. This is corroborated by the comparison with the values reported by Ghosh et al.[60] (18.512 Å^3/atom) or Zhang et al.[33] (18.347 Å^3/atom). The present result coincides almost exactly with the average of the previous ones.

Composition Dependence of EOF and E_{coh}

The effects on the EOF of the η'-$Cu_6(Sn,In)_5$ compounds of progressively replacing the Sn atoms at 4e, $8f_1$, $8f_2$, 4e + $8f_1$, and 4e + $8f_2$ sites by In are presented in Fig. 3a using symbols, whereas the dashed line describes the usual thermodynamic reference values corresponding to the linear interpolation between the EOF for the EMCs. The resulting EOF versus at.% In relation shows, in general, negative deviations from the reference line. It is also found that addition of In makes the ternary Cu–Sn–In compounds more stable than Cu_6Sn_5 for compositions up to 60 at.% In. The compounds with the lowest EOF, i.e., the most stable ones with respect to the EMCs, are compound VI (i.e., $Cu_{24}In_4Sn_8In_8$) and compound IV (i.e., $Cu_{24}Sn_4Sn_8In_8$). In both cases, the Sn atoms occupy the $8f_1$ sites whereas the In atoms are placed at the remaining sites (viz. the 4e sites, $8f_2$ sites, or both). The least stable phase with respect to the thermodynamic reference line is compound III (i.e., $Cu_{24}Sn_4In_8Sn_8$), where the In atoms are placed at $8f_1$ sites. Other compounds with In atoms at the $8f_1$ sites also present low thermodynamic stability, viz. compound V (i.e., $Cu_{24}In_4In_8Sn_8$) and compound VII (i.e., $Cu_{24}Sn_4In_8In_8$). In the following we compare the present findings with previously published results.

Ab initio EOF values for the η'-Cu_6Sn_5 phase were reported by Ref. 60 (−3.205 kJ/mol-atom) and Ref. 33 (−3.780 kJ/mol-atom). The present result (−3.35 kJ/mol-atom) falls in between.

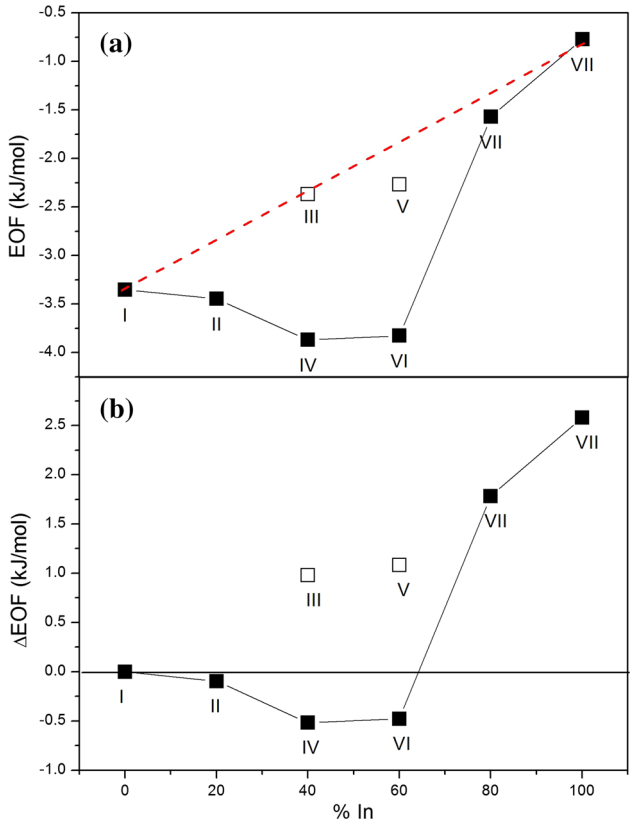

Fig. 3. (a) Composition dependence of energy of formation (EOF) from the elements of the (*mC44*) η'-$Cu_6(Sn,In)_5$ compounds, in kJ per mole of atoms (symbols). The thermodynamic reference line, corresponding to the linear interpolation between the EOF of the EMCs, is also indicated (dashed line). (b) Difference between the EOF of the ternary compounds and the EOF of the Cu_6Sn_5 EMC (symbols).

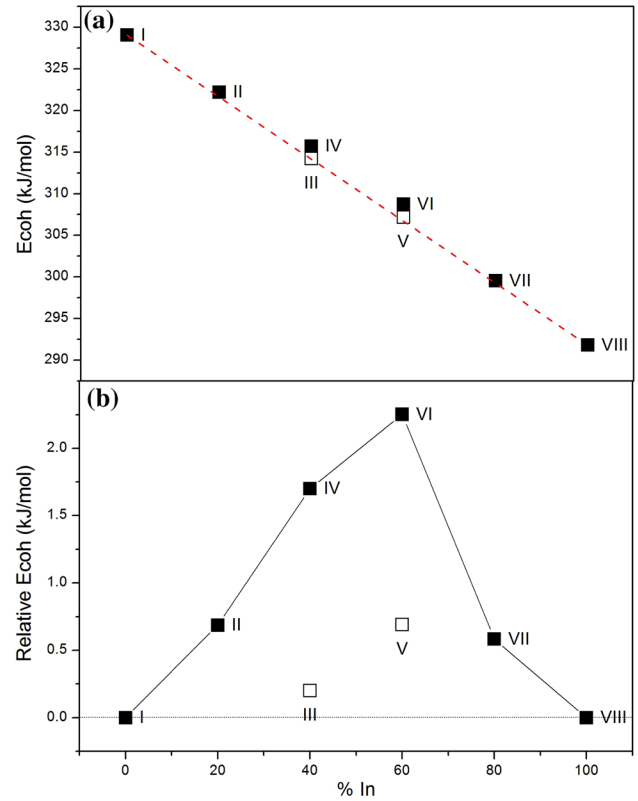

Fig. 4. (a) Composition dependence of cohesive energy (E_{coh}) of the (*mC44*) η'-$Cu_6(Sn,In)_5$ compounds. (b) Deviations of the current E_{coh} versus at.% In values from the linear interpolation between E_{coh} for the EMCs (symbols). The energy values are given in kJ per mole of atoms.

The only source of information on the EOF for η'-$Cu_6(Sn,In)_5$ compounds is the work by Zhang et al.[33] They studied the difference Δ(EOF) between the EOF values for the ternary compounds and the energy of formation of the binary η'-Cu_6Sn_5 phase, finding that Δ(EOF) is: (1) negative when the Sn atoms at Wyckoff positions 4e and $8f_2$ are replaced by In atoms, but (2) positive when Sn atoms at $8f_1$ sites are replaced by In. Unfortunately, their EOF values were not listed. The Δ(EOF) values obtained in the present work, plotted using symbols in Fig. 3b, are qualitatively consistent with the results by Zhang et al.[33] We remark that the energetic effects of substitution of Sn by In are further discussed in "Discussion" section.

The E_{coh} versus at.% In values for the current η'-$Cu_6(Sn,In)_5$ IMCs are presented in Fig. 4a using symbols. Two aspects of the current results can be highlighted.

In the first place, when passing from η'-Cu_6Sn_5 to η'-Cu_6In_5, the E_{coh} of the compounds decreases smoothly, deviating very little from the dashed line, which represents the values expected from a linear interpolation between E_{coh} for the EMCs. This general trend in the variation of E_{coh} between η'-Cu_6Sn_5 and η'-Cu_6In_5 is discussed in "Discussion" section in terms of the valence-electron density and changes in the number of interatomic bonds.

In the second place, we focus on the deviations of the current E_{coh} versus at.% In values from the linear interpolation between E_{coh} for the EMCs, as plotted in Fig. 4b using symbols. It is found that compounds VI (i.e., $Cu_{24}In_4Sn_8In_8$) and IV (i.e., $Cu_{24}Sn_4Sn_8In_8$)—where the stabilizing effect upon EOF of the replacement of Sn by In was largest (Fig. 3b)—show positive deviations of the order of 2 kJ/mol-atom from the dashed line. In "Discussion" section, the effect upon E_{coh} of the various possible substitutions of Sn by In is analyzed in a systematic fashion. On these bases, the stabilizing effects upon EOF will be discussed.

DISCUSSION

Effects of Electron Density and Interatomic Bonding on Cohesive Properties

As a first step in the development of a microscopic picture of the observed trends in the cohesive properties, we analyze the general trends in E_{coh} using two complementary accounts of the changes

occurring when In is incorporated into the crystal structure.

The first approach, recently presented by the current authors,[47] makes use of a variable related to the electron density in the material, which has its roots in a semiempirical model presented long ago by Miedema et al.[64] in the work by Moruzzi et al.,[65] Sigalas et al.,[66] and Gilman.[67] A thorough review of these bases has been reported elsewhere.[47] Here we only give the main points: (1) following Gilman et al.[67] we use the valence-electron density (n_{VED}) parameter describing the number of valence electrons per unit volume of the material; (2) n_{VED} was calculated by assuming for the elements the same number of valence electrons considered in the PAW calculations (viz. 11 valence electrons for Cu, 3 for In, and 4 for Sn); (3) in addition to stable IMCs, the results for metastable and nonstable (i.e., ideal or hypothetical) ones are included. On these bases, two linear correlations between combinations of the quantities V_0, B_0, and E_{coh}, and the n_{VED} parameter were previously established for binary Cu–Sn and Cu–In stoichiometric compounds.[47] These correlations will now be used to analyze the current results. The first correlation involves a linear variation of the parameter $(E_{coh})^{1/2}/V_0$ with n_{VED}, and the second correlation involves a linear variation of the parameter $(B_0/V_0)^{1/2}$, with n_{VED}. These are presented in Fig. 5a and b, respectively. In these graphics, the previous results for the Cu–Sn and Cu–In IMCs (empty symbols) and a linear fit to them (solid line) are compared with the present results (filled symbols). According to Fig. 5, the general trends in the variations in the cohesive properties of η'-$Cu_6(Sn,In)_5$ IMCs caused by the replacement of Sn by In, as shown in Fig. 4a, can be accurately interpreted in terms of the change in the concentration of valence electrons in this class of compounds.

The second approach, related to the classical bond-energy model, aims to describe the changes in the cohesive properties in terms of the variation in the number of interatomic bonds of type Cu–Cu, Cu–Sn, Cu–In, In–In, Sn–In, and Sn–Sn. Such an approach is applied in the following to the E_{coh} values of the η'-$Cu_6(Sn,In)_5$ compounds. To this end, the number of each kind of interatomic bond is represented by the respective number of nearest-neighbor bonding pairs (N_{X-Y}) (with X, Y = Cu, Sn, In) per unit cell. The results are plotted in Fig. 6. These plots suggest that the observed decrease in E_{coh} associated with the replacement of Sn by In cannot be related to the number of Cu–Cu bonds (Fig. 6c), which remains unchanged along compounds I to VII. Instead, such a decrease correlates very well with: (1) the decrease in the number of seemingly strong Cu–Sn (Fig. 6a) and Sn–Sn (Fig. 6d) bonds, (2) the increase in the number of seemingly weaker Cu–In (Fig. 6b) and In–In (Fig. 6e) bonds, and (3) the increase first then the decrease in the number of Sn–In bonds occurring when passing from Cu_6Sn_5 (compound I) to Cu_6In_5 (compound VIII) (Fig. 6f).

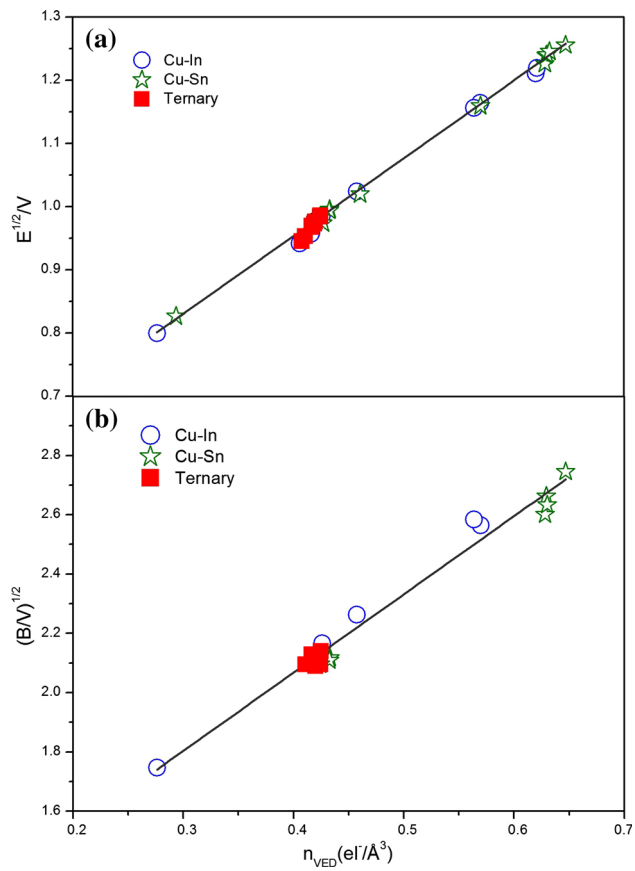

Fig. 5. Cohesion-related properties: (a) $(E_{coh})^{1/2}/V_0$ and (b) $(B_0/V_0)^{1/2}$, of the η'-$Cu_6(Sn,In)_5$ IMCs as a function of the valence-electron density parameter (n_{VED}).

The picture of the general trends in the variation of cohesive properties arrived at in the present section will be further developed in the remainder of this paper by considering two additional aspects, namely the energy effects associated with the incorporation of In at specific crystallographic sites ("Effects of Crystallographic Site Occupation on Cohesion and Phase Stability" section) and the electron band structure interpretation of the bonding trends ("Electron Band Structure Interpretation of the Bonding Trends" section).

Effects of Crystallographic Site Occupation on Cohesion and Phase Stability

Recent *ab initio* studies considered the energy effects involved in placing atoms of a third element at various Wyckoff sites of the η'-Cu_6Sn_5 phase.[32,33] In "Composition Dependence of EOF and E_{coh}" section, a preliminary qualitative analysis was performed, by referring to Figs. 3b and 4b. In the following, the effects on E_{coh} of substituting the Sn atoms placed at 4e, $8f_1$, and $8f_2$ sites by In will be further investigated. To this end, various differences of the type $\Delta E^{4e}_{coh}(j/k)$,

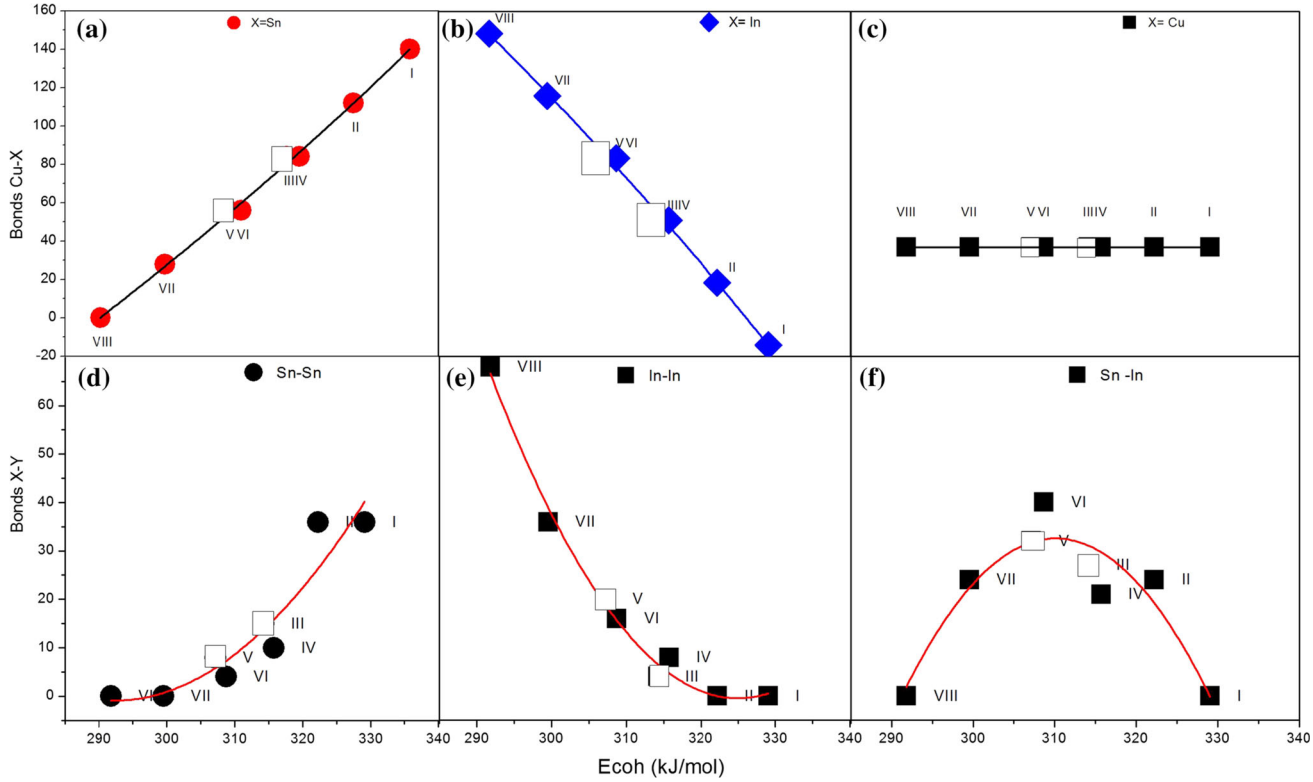

Fig. 6. Cohesive energy versus number of nearest-neighbor bonding pairs (N_{X-Y}) (with X, Y = Cu, Sn, In) per unit cell. (a) Cu–Sn, (b) Cu–In, (c) Cu–Cu, (d) Sn–Sn, (e) In–In, (f) Sn–In, bonding pairs.

$\Delta E^{8f1}_{coh}(j/k)$, and $\Delta E^{8f2}_{coh}(j/k)$ between the cohesive energy of the compounds with j/k = I to VIII were calculated. For instance, the difference ΔE^{4e}_{coh}(II/I), describing the effect of full Sn-by-In substitution at 4e sites, was obtained as [$E_{coh}(Cu_{24}In_4Sn_8Sn_8) - E_{coh}(Cu_{24}Sn_4Sn_8Sn_8)$], the difference ΔE^{8f1}_{coh}(III/I) corresponding to the $8f_1$ sites as [$E_{coh}(Cu_{24}Sn_4In_8Sn_8) - E_{coh}(Cu_{24}Sn_4Sn_8Sn_8)$], and the difference ΔE^{8f2}_{coh}(VI/I) involving the $8f_2$ sites as [$E_{coh}(Cu_{24}Sn_4Sn_8In_8) - E_{coh}(Cu_{24}Sn_4Sn_8Sn_8)$]. These and the remaining $\Delta E_{coh}(j/k)$ differences, obtained by proceeding in an analogous way, are listed in Table II and plotted in Fig. 7 using symbols.

The present results indicate that replacement of Sn atoms by In atoms involves a loss in E_{coh} of the compound, which in magnitude is: (1) largest when 8 In atoms are placed at $8f_1$ sites (viz. about −16 kJ/mol-atom), (2) somewhat lower when 8 In atoms are placed at the $8f_2$ sites (viz., about −14 kJ/mol-atom), and (3) lowest when 4 In atoms are placed at the 4e sites (viz. about −7 kJ/mol-atom). On this basis, it is possible to develop a qualitative interpretation of the key features of the EOF versus at.% In relation presented in Fig. 3, as follows: (a) the most stable compounds are those without In at the $8f_1$ sites; (b) progressive incorporation of In at the 4e sites (as in compound II), the $8f_2$ sites (as in compound IV), or both (as in compound VI) does not crucially affect their relative stability; (c) incorporation of In at the $8f_1$ sites (as in compound III) or both the 4e and $8f_1$ sites (as in compound V) involves a significant decrease in thermodynamic stability. We emphasize that the trends in the stabilizing effects expressed by Zhang et al.[33] in terms of Δ(EOF), mentioned in "Composition Dependence of EOF and E_{coh}" section and discussed by referring to Fig. 3b, can also be understood with reference to the current systematics of $\Delta E_{coh}(j/k)$ differences.

Electron Band Structure Interpretation of the Bonding Trends

To analyze how the In additions to the η'-Cu_6Sn_5 phase influence the electronic properties, we plot in Fig. 8a–e the total (DOS) and projected (PDOS) electronic density of states for the Cu_6Sn_5 (I) and Cu_6In_5 (VIII) EMCs, and the compounds II, IV, and VI, which are the most stable ones when In is incorporated into the lattice. The total DOS of a system describes the number of states per interval of energy at each energy level available to be occupied, while the PDOS is the decomposition of the total DOS according to the different atomic (Cu, In, and Sn) and angular momentum (s, p, and d) contributions. As discussed in our previous works, there are two main contributions to the electronic structure for this class of compounds.[47] One is the interaction between the Cu atoms through their atomic d-electron orbitals, which determines the main bonding band of the DOS and leads to the

Table II. Decrease in cohesive energy associated with replacement of Sn atoms occupying 4e, $8f_1$, and $8f_2$ Wyckoff sites by In in η'-Cu_6Sn_5 phase

ΔE^{4e}(II/I)	ΔE^{8f1}(III/I)	ΔE^{8f2}(IV/I)
−6.840	−14.851	−13.352
ΔE^{4e}(V/III)	ΔE^{8f1}(VII/IV)	ΔE^{8f2}(VII/III)
−7.038	−16.170	−14.671
ΔE^{4e}(VI/IV)	ΔE^{8f1} (V/II)	ΔE^{8f2}(VI/II)
−6.977	−15.049	−13.489
ΔE^{4e}(VIII/VII)	ΔE^{8f1}(VIII/VI)	ΔE^{8f2}(VIII/V)
−7.734	−16.928	−15.368

The cohesive energy differences $\Delta E^{4e}_{coh}(j/k)$, $\Delta E^{8f1}_{coh}(j/k)$, and $\Delta E^{8f2}_{coh}(j/k)$ (with j, k = I to VIII) between E_{coh} of the compounds in Table I are defined in the text. The values are given in kJ/mol-atom.

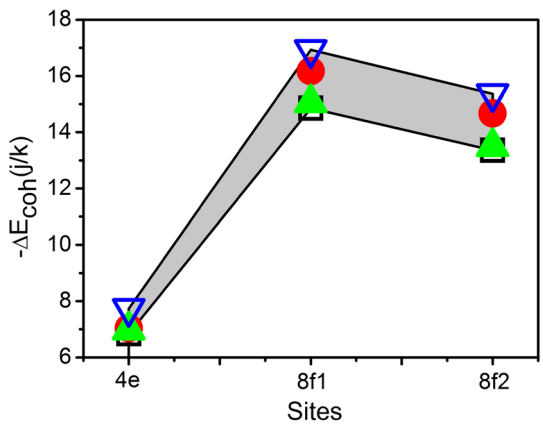

Fig. 7. Decrease in cohesive energy (in kJ/mol-atom) associated with replacement of Sn atoms occupying 4e, $8f_1$, and $8f_2$ Wyckoff sites by In in η'-Cu_6Sn_5 phase. The cohesive energy differences $\Delta E^{4e}_{coh}(j/k)$, $\Delta E^{8f1}_{coh}(j/k)$, and $\Delta E^{8f2}_{coh}(j/k)$ (with j, k = I to VIII) between E_{coh} of the compounds are defined in the text, listed in Table I, and plotted using symbols. Each type of symbol is used to represent the $\Delta E^{4e}_{coh}(j/k)$, $\Delta E^{8f1}_{coh}(j/k)$, and $\Delta E^{8f2}_{coh}(j/k)$ values given in each row of Table I. The solid lines are only guides to the eye. The dashed area indicates the scatter band of the $\Delta E^{4e}_{coh}(j/k)$, $\Delta E^{8f1}_{coh}(j/k)$, and $\Delta E^{8f2}_{coh}(j/k)$ (with j, k = I to VIII) values.

largest contribution to the cohesive energy. Figure 8 shows that the shape of the total DOS practically coincides with the Cu-d PDOS. The second contribution to cohesion in this type of compound comes from covalent hybridization of the d-atomic states of Cu with the In p- and Sn p-states. An additional observation regarding the DOS for this type of compound is that the lowest-energy occupied states originate from s-states of In and Sn. These general features are present in the DOS of the $Cu_6(Sn,In)_5$ compounds studied here (Fig. 8).

The DOS for the Cu_6Sn_5 EMC, reproduced here from Ref. 40 (Fig. 8a), shows the main d bonding band extending from approximately −5 eV to −2 eV; on its left side, these d-states superpose with a minor contribution of Sn p-states extending from around −6 eV to −3 eV. At lower energies, and separated by a pseudogap, the Sn s-states, extending from approximately −11 eV to −6 eV, are the ones that mainly determine the DOS. When In is added to the compound, this general picture of the DOS remains qualitatively unchanged (Fig. 8b–e). However, there are some differences to be noted. As the In content in the compound increases, the occupied bandwidth decreases from 11 eV to 9.5 eV, for the Cu_6Sn_5 and Cu_6In_5 EMC, respectively. The Cu d-states, which dominate the main contribution to the total DOS, remain located within −5 eV to −2 eV, with their bandwidths and locations practically unaffected by increased addition of In. This observation is related to the fact that the number of Cu–Cu bonds does not change when increasing the In content in the ternary IMCs, as discussed in "Effects of Electron Density and Interatomic Bonding on Cohesive Properties" section. This effect seems to be dominant in spite of the fact that the overall volume reduction (Fig. 2) would lead to an increase in the bandwidth.

The contributions of the In s- and p-states to the DOS behave similarly to those of Sn in the Cu_6Sn_5 compound. An important aspect to mention is that, with incorporation of In into the lattice, the s- and p-bands of both In and Sn shift to higher energies, resulting in more efficient overlap with the Cu d-states. This is expected to yield a stronger p–d stabilizing hybridization effect. Indeed, this effect could in principle explain the stabilizing effect upon the EOF of the replacement of Sn by In, for In contents lower than 60 at.%. However, due to the decrease in the number of valence electrons from Sn (4) to In (3), the net p-band contribution reduces in intensity as the In content is increased. In turn, this effect could explain the smooth decrease in E_{coh} as In atoms replace Sn atoms in the Cu_6Sn_5 compound, as well as the correlations discussed in "Effects of Electron Density and Interatomic Bonding on Cohesive Properties" section. The above-mentioned p–d hybridization contribution effect to bonding can, at the same time, be correlated with the positive deviations of E_{coh} from the values expected from a linear interpolation between the values for the EMCs, as shown in Fig. 4b. In summary, these two opposite effects can explain the relative loss in stability of the ternary IMCs at sufficiently high In content, thus accounting for the general trends in

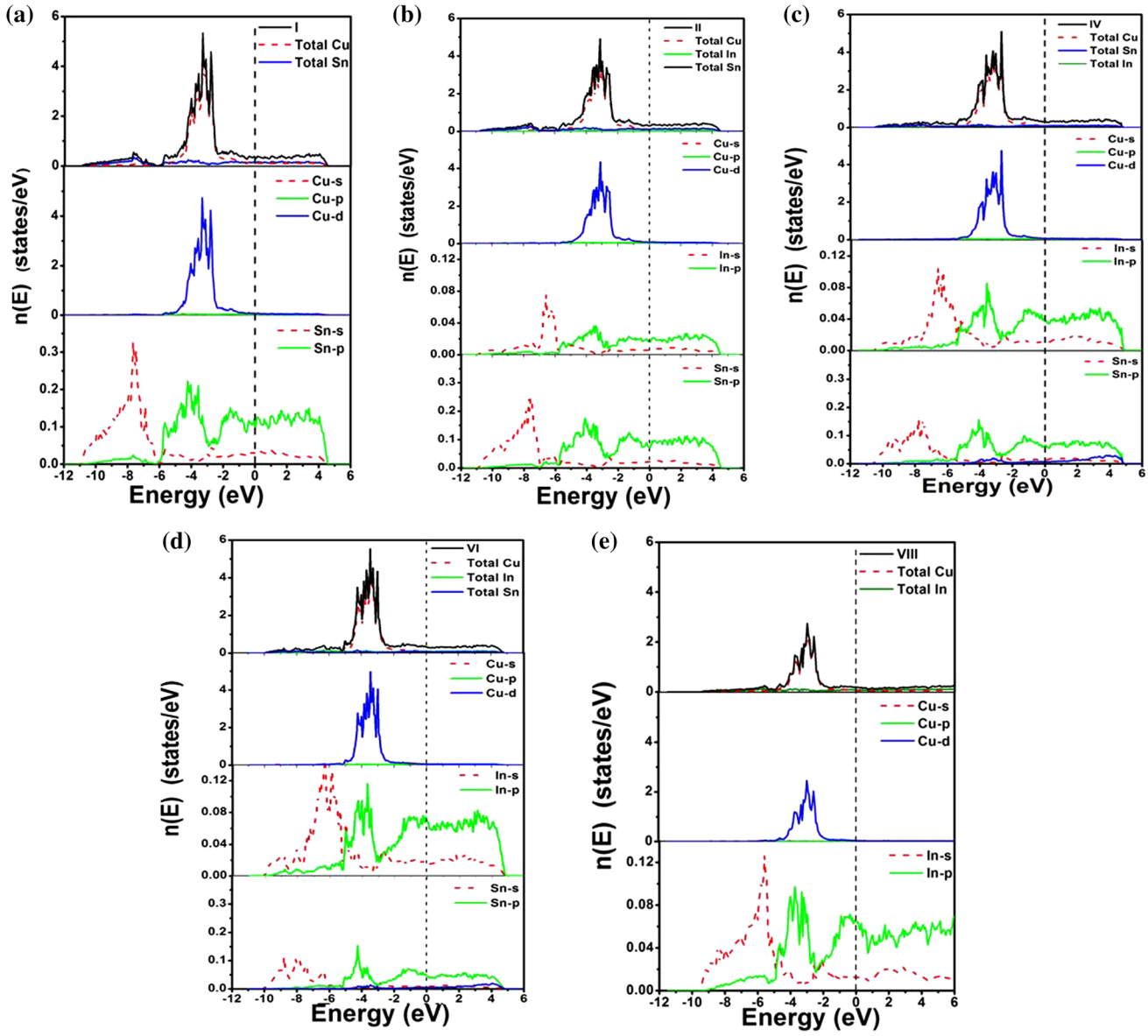

Fig. 8. Total and projected DOS for compounds (a) $Cu_{24}Sn_{20}$ (I), (b) $Cu_{24}In_4Sn_8Sn_8$ (II), (c) $Cu_{24}Sn_4Sn_8In_8$ (IV), (d) $Cu_{24}In_4Sn_8In_8$ (VI), and (e) $Cu_{24}In_{20}$ (VIII). The atomic decomposed PDOS with their angular momentum (*s*, *p*, and *d*) band contributions, are plotted. The origin of the energy scale corresponds to the Fermi level.

thermodynamic stability when Sn atoms are replaced by In atoms.

CONCLUSIONS

Current Work

The rapid development of low-melting, lead-free soldering technology has motivated increased interest in the structural, mechanical, and phase stability properties of the intermetallic compounds formed in Cu/In-Sn/Cu joints. A first-principles characterization of the family of compounds formed by progressively replacing all Sn atoms of the (*mC44*) η'-Cu_6Sn_5 phase by In atoms is reported herein. The work involves *ab initio* calculations of the composition dependence of the structural, thermodynamic, and cohesion-related properties of the ternary η'-$Cu_6(Sn,In)_5$ compounds.

The current results are discussed by combining two approaches to the analysis of the thermophysics of intermetallic phases. The first approach aims at correlating the main variations of the cohesive properties with: (1) the valence-electron density, (2) the number of Cu–Sn and Cu–In bonding pairs, and (3) the variations in the intensity of the *d*-electron bonding and *p*–*d* hybridization effects. The second approach aims at comparing the energy effects of incorporating In atoms at specific Wyckoff sites of the (*mC44*) η'-Cu_6Sn_5 structure.

The key conceptual result of the paper is that, by combining these two approaches, it is possible to develop a rather complete picture of the overall thermodynamic and bonding trends and the specific effects of substituting Sn by In at relevant Wyckoff positions.

Additional Theoretical and Experimental Work

The results for the η'-$Cu_6(Sn,In)_5$ compounds reported herein add to the database of fundamental information necessary to gain understanding of the experimental trends in cohesion-related properties. However, it is evident that further studies are necessary to: (1) test the present predictions, and (2) make even more direct contact with current research issues, such as the reliability and performance of solder joints, particularly in devices and systems of interest in microelectronics and solar photovoltaic technologies subjected to mechanical loading.

Concerning item (1), it is suggested that measurement of the volume per atom and the bulk modulus of single-phase η'-Cu_6Sn_5 alloys with varying In contents would offer a direct way to corroborate the predictions of the present study.

Concerning item (2), we consider that the significant advances currently being made in experimental elucidation of the following issues, should be taken into account as a horizon and benchmark for design of future experimental work: (a) the microstructural evolution and damage mechanisms affecting the reliability and performance in a variety of such systems;[24–29] (b) the characterization of technologically relevant cohesion, adhesion, and debonding parameters;[68–70] and (c) the study of the small-scale mechanical properties of metallic systems.[71–75] In relation to such advances, characterization of the brittleness and other properties involved in crack formation and propagation in η'-Cu_6Sn_5 compounds should be considered as highly relevant experimental topics.

Finally, some issues emerge as key targets for additional theoretical work on the η'-Cu_6Sn_5 phases. In particular, it seems necessary to establish the composition dependence of: (I) the thermal expansion coefficients and their effects upon the thermal stresses, and (II) the engineering elastic constants (shear modulus, elastic modulus, and Poisson's ratio). Moreover, the possible use of such constants in developing system-specific correlations appropriate for systematizing and predicting mechanical behavior should also be explored. Additional work along these lines is in progress in our research group.

ACKNOWLEDGEMENTS

This work was supported by Project PIP 112-20110100814 from Consejo Nacional de Investigaciones Científicas y Técnicas (CONICET) and Project I197 from Universidad Nacional del Comahue.

REFERENCES

1. H.R. Kotadia, P.D. Howes, and S.H. Mannan, *Microelectron. Reliab.* 54, 1253 (2014).
2. J.L. Freer and J.W. Morris, *J. Electron. Mater.* 21, 647 (1992).
3. T. Laurila, V. Vuorinen, and J.K. Kivilahti, *Mater. Sci. Eng., R* 49, 1 (2005).
4. P.-E. Tegehall, Review of the impact of intermetallic layers on the brittleness of tin-lead and lead-free solder joints. (IVF Project Report 06/07, © IVF Industrial Research and Development Corporation, Sweden), http://extra.ivf.se/eqs/dokument/7%20pet6005.pdf. Accessed 15 Dec 2016.
5. K.N. Tu, *Acta Metall. Mater.* 21, 347 (1973).
6. K.N. Tu and R.D. Thompson, *Acta Metall. Mater.* 30, 947 (1982).
7. K.N. Tu, *Mater. Chem. Phys.* 46, 217 (1996).
8. H.L.J. Pang, K.H. Tan, X.Q. Shi, and Z.P. Wang, *Mater. Sci. Eng.* A307, 42 (2001).
9. T.H. Chuang, C.L. Yu, S.Y. Chang, and S.S. Wang, *J. Electron. Mater.* 31, 640 (2002).
10. S.S. Wang, Y.H. Tseng, and T.H. Chuang, *J. Electron. Mater.* 35, 165 (2006).
11. R. Labie, W. Ruythooren, and J. Van Humbeeck, *Intermetallics* 15, 396 (2007).
12. B.-J. Kim, G.-T. Lim, J. Kim, K. Lee, Y.-B. Park, H.-Y. Lee, and Y.-C. Joo, *J. Electron. Mater.* 39, 2281 (2010).
13. Y.W. Wang, Y.W. Lin, and C.R. Kao, *J. Alloys Compd.* 493, 233 (2010).
14. J.-M. Park, S.-H. Kim, M.-H. Jeong, and Y.-B. Park, *Jpn. J. Appl. Phys.* 53, 05HA06 (2014).
15. Y. Li, A.B.Y. Lim, K. Luo, Z. Chen, F. Wu, and Y.C. Chan, *J. Alloys Compd.* 673, 372 (2016).
16. A.K. Larsson, L. Stenberg, and S. Lidin, *Acta Cryst.* B50, 636 (1994).
17. J.D. Bernal, *Nature* 122, 54 (1928).
18. Y.Q. Wu, J.C. Barry, T. Yamamoto, Q.F. Gu, S.D. McDonald, S. Matsumura, H. Huang, and K. Nogita, *Acta Mater.* 60, 6581 (2012).
19. G. Zeng, S.D. McDonald, Q. Gu, S. Suenaga, Y. Zhang, J. Chen, and K. Nogita, *Intermetallics* 43, 85 (2013).
20. E. Nagy, F. Kristaly, A. Gyenes, and Z. Gacsi, *Arch. Metall. Mater.* 60, 1511 (2015).
21. B. Vandevelde, M. Gonzalez, P. Limaye, P. Ratchev, and E. Beyne, *Microelectron. Reliab.* 47, 259 (2007).
22. T.T. Mattila and J.K. Kivilahti, *J. Electron. Mater.* 34, 969 (2005).
23. L. Jiang, N. Muthegowda, M.A. Bathia, A. Migliori, K.N. Solanki, and N. Chawla, *Scripta Mater.* 107, 26 (2015).
24. A.S. Budiman, G. Illya, V. Handara, W.A. Caldwell, C. Bonelli, M. Kunz, N. Tamura, and D. Verstraeten, *Sol. Energy Mater. Sol. C* 130, 303 (2014).
25. I. Radchenko, S.K. Tippabhotla, N. Tamura, and A.S. Budiman, *J. Electron. Mater.* 45, 6222 (2016).
26. H.-A.-S.S. Shin, B.-J. Kim, J.-H. Kim, S.-H. Hwang, A.S. Budinam, H.-Y. Son, K.-Y. Byun, N. Tamura, M. Kunz, D.-I. Kim, and Y.-C. Joo, *J. Electron. Mater.* 41, 712 (2012).
27. K.N. Rengarajan, I. Radchenko, G. Illya, V. Handara, M. Kunz, N. Tamura, and A.S. Budiman, *Procedia Eng.* 139, 76 (2016).
28. S.K. Tippabhotla, I. Radchenko, K.N. Rengarajan, G. Illya, V. Handara, M. Kunz, N. Tamura, and A.S. Budiman, *Procedia Eng.* 139, 123 (2016).
29. T. Tian, R. Morusupalli, H. Shin, H.-Y. Son, K.-Y. Byun, Y.-C. Joo, R. Caramto, L. Smith, Y.-L. Shen, M. Kunz, N. Tamura, and A.S. Budiman, *Procedia Eng.* 139, 101 (2016).
30. K. Nogita and T. Nishimura, *Scripta Mater.* 59, 191 (2008).
31. G. Zeng, S.D. McDonald, Q. Gu, Y. Terada, K. Uesugi, H. Yasuda, and K. Nogita, *Acta Mater.* 83, 357 (2015).

32. F. Gao, J. Qu, and T. Takemoto, *J. Electron. Mater.* 39, 426 (2010).
33. Y. Zhang, D. Yuan, J. Chen, G. Zeng, T. Fan, Z. Liu, C. Wu, and L. Liu, *J. Electron. Mater.* 45, 4018 (2016).
34. W. Köster, T. Gödecke, and D. Heine, *Z. Metallkd.* 63, 802 (1972).
35. G. Aurelio, S. Sommadossi, and G. Cuello, *J. Appl. Phys.* 112, 053520 (2012).
36. G. Aurelio, S. Sommadossi, and G. Cuello, *J. Electron. Mater.* 41, 3223 (2012).
37. D. Kim and S. Jung, *J. Alloys Compd.* 386, 151 (2005).
38. S. Sommadossi and A. Fernández Guillermet, *Intermetallics* 15, 912 (2007).
39. I. Ansara, T.G. Chart, A. Fernández Guillermet, F.H. Hayes, U.R. Kattner, D.G. Pettifor, N. Saunders, and K. Zeng, *Calphad* 21, 171 (1997).
40. S. Ramos de Debiaggi, C.D. Toro, G. Cabeza, and A. Fernández Guillermet, *J. Alloys Compd.* 542, 280 (2012).
41. S. Ramos de Debiaggi, G.F. Cabeza, C.D. Toro, A.M. Monti, S. Sommadossi, and A. Fernández Guillermet, *J. Alloys Compd.* 509, 3238 (2011).
42. C.D. Toro, S. Ramos de Debiaggi, and A.M. Monti, *Phys. B* 407, 3236 (2012).
43. S. Ramos de Debiaggi, C.D. Toro, G.F. Cabeza, and A. Fernández Guillermet, *J. Alloys Compd.* 576, 302 (2013).
44. G. Kresse and J. Joubert, *Phys. Rev. B* 59, 1758 (1999).
45. P.E. Blöchl, *Phys. Rev. B* 50, 17953 (1994).
46. G. Kresse and J. Furthmüller, *Comput. Mater. Sci.* 6, 15 (1996).
47. S.B. Ramos, N.V. González Lemus, G.F. Cabeza, and A. Fernández Guillermet, *J. Phys. Chem. Sol.* 93, 40 (2016).
48. S. Ramos de Debiaggi, N.V. González Lemus, C.D. Toro, and A. Fernández Guillermet, *J. Alloys Compd.* 619, 464 (2015).
49. J.P. Perdew and Y. Wang, *Phys. Rev. B* 45, 13244 (1992).
50. H.J. Monkhorst and J.D. Pack, *Phys. Rev. B* 13, 5188 (1976).
51. M. Methfessel and A.T. Paxton, *Phys. Rev. B* 40, 3616 (1986).
52. R.A. Evarestov, *Quantum Chemistry of Solids: The LCAO First Principles Treatment of Crystals* (Berlin: Springer, 2007).
53. P. Villars, *Pearson's Handbook Desk Edition* (Materials Park: ASM International, 1997).
54. K. Takemura, *Phys. Rev. B* 44, 545 (1991).
55. M.E. Straumanis and L.S. Yu, *Acta Crystallogr. A* 25A, 676 (1969).
56. M. Kamtola and E. Tokola, *Physics* 223A, 1 (1967).
57. W.C. Overton Jr. and J. Gaffney, *Phys. Rev.* 98, 969 (1955).
58. D.J. Steinberg, *J. Phys. Chem. Solids* 43, 1173 (1982).
59. J.A. Rayne and B.S. Chandrasekhar, *Phys. Rev.* 120, 1658 (1960).
60. G. Ghosh and M. Asta, *J. Mater. Res.* 20, 3102 (2005).
61. H. Okamoto and T.B. Massalski, *J. Phase Equilib.* 15, 500 (1994).
62. L. Kaufman and H. Bernstein, *Computer Calculation of Phase Diagrams* (New York: Academic, 1970).
63. M. Hillert, *Phase Equilibria, Phase Diagrams and Phase Transformations* (Cambridge: Cambridge University Press, 1998).
64. A.R. Miedema, F.R. de Boer, and P.F. de Chatel, *J. Phys. F: Metal. Phys.* 3, 1558 (1973).
65. V.L. Moruzzi, J.F. Janak, and A.R. Williams, *Calculated Electronic Properties of Metals* (New York: Pergamon, 1978).
66. M. Sigalas, J.H. Rose, D.A. Papaconstantopoulos, and H.B. Shore, *Phys. Rev. B* 58, 13438 (1998).
67. J.J. Gilman, R.W. Cumberland, and R.B. Kaner, *Int. J. Refract. Met. Hard Mater.* 24, 1 (2006).
68. R. Shivakumar, S.K. Tippabhotla, V.A. Handarab, G. Illya, A.A.O. Taya, F. Novoa, R.H. Dauskardt, and A.S. Budiman, *Procedia Eng.* 139, 47 (2016).
69. S.R. Dupont, E. Voroshazi, D. Nordlund, and R.H. Dauskardt, *Sol. Energy Mater. Sol. C* 132, 443 (2015).
70. F.D. Novoa, D.C. Miller, and R.H. Dauskardt, *Sol. Energy. Mater. Sol. C* 120, 87 (2014).
71. A.S. Budiman, S.-M. Han, N. Li, Q.-M. Wei, P. Dickerson, N. Tamura, M. Kunz, and A. Misra, *J. Mater. Res.* 27, 599 (2012).
72. G. Lee, M.J. Burek, D. Jang, S.-M.J. Han, N. Tamura, M. Kunz, J.R. Greer, and T.Y. Tsui, *Mater. Sci. Eng., A* 538, 89 (2012).
73. A.S. Budiman, K.R. Narayanan, N. Li, J. Wang, N. Tamura, M. Kunz, and A. Misra, *Mater. Sci. Eng., A* 635, 6 (2015).
74. G. Lee, J.-Y. Kim, A.S. Budiman, N. Tamura, M. Kunz, K. Chen, M.J. Burek, J.R. Greer, and T.Y. Tsui, *Acta Mater.* 58, 1361 (2010).
75. Y. Kim, A.S. Budiman, J.K. Baldwin, N.A. Mara, A. Misra, and S.M. Han, *J. Mater. Res.* 27, 592 (2012).